

On the valence-bond solid phase of the crossed-chain quantum spin model

Wolfram Brenig and Matthias Grzeschik

Institut für Theoretische Physik, Technische Universität Braunschweig, 38106 Braunschweig, Germany

(Dated: October 22, 2018)

Using a series expansion based on the flow-equation method we study the ground state energy and the elementary triplet excitations of a generalized model of crossed spin-1/2 chains starting from the limit of decoupled quadrumer. The triplet dispersion is shown to be very sensitive to the inter-quadrumer frustration, exhibiting a line of almost complete localization as well as lines of quantum phase transitions limiting the stability of the valence-bond solid phase. In the vicinity of the checkerboard-point a finite window of exchange couplings is found with a non-zero spin-gap, consistent with known results from exact diagonalization. The ground state energy is lower than that of the bare quadrumer case for all exchange couplings investigated. In the limiting situation of the fully frustrated checkerboard magnet our results agree with earlier series expansion studies.

PACS numbers: 75.10.Jm, 75.50.Ee, 75.40.-s

I. INTRODUCTION

Frustrated quantum magnets have attracted considerable interest recently. On the one hand this is related to the ongoing quest for systems exhibiting spin liquid behavior and quantum disorder¹. On the other hand numerous materials displaying geometrical or quantum chemical frustration of the magnetic exchange have been discovered recently. Prominent examples are the one-dimensional (1D) frustrated spin-Peierls compound CuGeO₃² or the 2D orthogonal spin-dimer system SrCu₂(BO₃)₂ with frustrating inter-dimer coupling³ as well as the 3D tetrahedral tellurate compounds Cu₂Te₂O₅X₂, with X=Cl, Br^{4,5}. One promising route into spin-liquid behavior is via the coupling of locally frustrated units like triangles or tetrahedra, as in the kagomé, the pyrochlore, and the checkerboard (i.e. planar pyrochlore) lattices. Both, on the kagomé and the checkerboard lattice low-lying singlets seem to exist with no long-range magnetic order (LRO) in the former^{6,7}, and a valence-bond-crystal (VBC) ground state in the latter case^{8,9,10,11}. The physics of the 3D pyrochlore quantum-magnet is still far from clarified with a hope that analysis of the planar model may lead to further progress in three dimensions^{12,13,14,15}.

A closely related approach to spin-liquids above one dimensions has become of interest recently based on the frustrated coupling of spin-1/2 Heisenberg chains to form the planar crossed-chain model (CCM)^{16,17,18}. A generalized version of this is depicted in fig. 1 which resembles the generic CCM for $j_0=j_1$. The generic CCM interpolates between three rather distinct regimes. Due to the complete frustration of the inter-chain exchange at $j_0=j_1$ and for $j_2/j_1 \gtrsim 1.25$, it has been argued that the CCM stabilizes a 2D 'sliding Luttinger liquid' (SLL)^{16,17,18}. This is in contrast to the instability of coupled Heisenberg chains with respect to spinon-binding and the formation of antiferromagnetism (AFM) or VBC order if linked via *non*-frustrating exchange. The SLL shows no LRO with massless, deconfined spinons forming the elementary excitations. At $j_0=j_1=j_2$ the

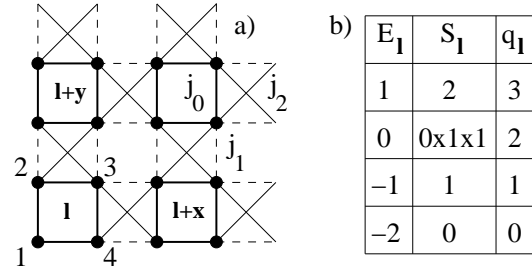


FIG. 1: a) The generalized crossed-chain model. Spin-1/2 moments are located on the solid circles. Thin solid(Thick solid and thin dashed) lines refer to the crossed chains(inter-chain coupling). The generic model with complete frustration of the inter chain coupling occurs at $j_0=j_1$. The quadrumer exchange is set to $j_0=1$ hereafter with j_1 and j_2 corresponding to the expansion parameters. b) Local energy E_I , total spin S_I , and quantum-number q_I of a single quadrumer.

CCM is identical to the checkerboard magnet exhibiting the aforementioned VBC ground state and a spin gap^{8,9,10,11}. Finally, for $j_2 \rightarrow 0$ and $j_0=j_1$ the CCM maps onto the 2D spin-1/2 Heisenberg model on the square-lattice with AFM LRO and gapless magnon excitations. The AFM LRO in the latter region and the VBC have been suggested to coexist in the vicinity of the point $j_2/j_1 \sim 0.7$ ^{19,20}, which however has been questioned based on results from exact diagonalization (ED)¹¹.

The CCM is under intense current investigation. The SLL limit has been analyzed by bosonization^{16,17,18}. Numerical studies have been performed on up to 36 spins^{8,9,11,21}. In particular, ED for $j_0=j_1$ in ref.¹¹ suggests the VBC spin-gap to close below $j_2/j_1 \lesssim 0.65$ and moreover 1D, i.e. SLL, behavior is found above $j_2/j_1 \gtrsim 1.5$. Several analytical methods have been employed, including various semiclassical, Sp(N), and linear-spin-wave (LSW) approaches incorporating $1/S$ -corrections also^{10,22,23,24,25}. LSW predicts stability of the AFM LRO for $j_2/j_1 \leq 0.76$ at $j_0=j_1$ and spin-1/2²². Because it is not even obvious that extrapolations from the large- S or $-N$ limit will lead to conclusive answers

for the quantum case, it seems highly desirable to obtain results from other analytic approaches applicable to $S=1/2$, such as eg. series expansions (SE). At $j_1=j_2$ SE has been performed starting from the quadrumer⁹ and the tetrahedral²⁶ limit. However, SE for $j_1 \neq j_2$ is not available.

In this context it is the purpose of this work to shed more light onto the quantum CCM by studying its elementary excitations, the stability of the VBC phase, and the ground state properties. This will be done by series expansions starting from the limit of decoupled quadrumeres. The paper is organized as follows. In section two we describe our method of calculation. In section three and four we discuss the triplet excitations and the instabilities of the VBC phase with respect to triplet softening. Section five is devoted to the ground state energy. A summary and some technical details are provided in the conclusions and the appendix.

II. SERIES EXPANSION BY CONTINUOUS UNITARY TRANSFORMATION

Recently it has been shown, that the checkerboard point of the CCM, i.e. $j_1=j_2=1$, can be described by SE in terms of the single coupling constant $j=j_1=j_2$, starting from the limit of decoupled quadrumeres⁹. The SE was found to adiabatically connect the bare VBC at $j=0$ to a renormalized one at $j=1$ without being hindered by quantum phase transitions. This is consistent with other findings of a VBC at $j_1=j_2=1$ ^{8,10,11}. Motivated by this we decompose the Hamiltonian of the CCM in a form adapted to a VBC symmetry breaking and normalized to the overall unit of energy j_0 which will be set equal to unity hereafter

$$H = \sum_{\mathbf{l}} \left[\sum_{i=1 \dots 4} \mathbf{S}_{i\mathbf{l}} \mathbf{S}_{i+1\mathbf{l}} + j_1 (\mathbf{S}_{2\mathbf{l}} \mathbf{S}_{1\mathbf{l}+\mathbf{y}} + \mathbf{S}_{3\mathbf{l}} \mathbf{S}_{4\mathbf{l}+\mathbf{y}} + \mathbf{S}_{3\mathbf{l}} \mathbf{S}_{1\mathbf{l}+\mathbf{x}} + \mathbf{S}_{4\mathbf{l}} \mathbf{S}_{2\mathbf{l}+\mathbf{x}}) + j_2 (\mathbf{S}_{2\mathbf{l}} \mathbf{S}_{4\mathbf{l}+\mathbf{y}} + \mathbf{S}_{3\mathbf{l}} \mathbf{S}_{1\mathbf{l}+\mathbf{y}} + \mathbf{S}_{3\mathbf{l}} \mathbf{S}_{1\mathbf{l}+\mathbf{x}} + \mathbf{S}_{4\mathbf{l}} \mathbf{S}_{2\mathbf{l}+\mathbf{x}}) \right] \quad (1)$$

$$= H_0 + \sum_{n=-N}^N (j_1 T_{1n} + j_2 T_{2n}) \quad (2)$$

$\mathbf{S}_{i\mathbf{l}}$ refers to spin-1/2 operators residing on the vertices $i=1 \dots 4$ of the quadrumer at site \mathbf{l} with periodic boundary conditions on i , c.f. fig. 1a). H_0 is the sum over local quadrumer Hamiltonians the spectrum of which, c.f. fig. 1b), consists of four equidistant levels which can be labeled by the local total spin $S_{\mathbf{l}}$ and a number of local energy quanta $q_{\mathbf{l}}$. H_0 displays an equidistant ladder spectrum labeled by $Q = \sum_{\mathbf{l}} q_{\mathbf{l}}$. The $Q=0$ sector is the *unperturbed* ground state $|0\rangle$ of H_0 , which is a VBC of quadrumer-singlets. The $Q=1$ -sector of H_0 consists of linear combinations of local $S_{\mathbf{l}}=1$ single-particle excitations of the VBC with $q_{\mathbf{l}}=1$, where \mathbf{l} runs over the lattice. At $Q=2$ the spectrum of H_0 has total spin $S=0,1$, or 2

and is of multiparticle nature. Eg., for total $S=0$ at $Q=2$ it comprises of one-particle singlets with $q_{\mathbf{l}}=2$ and two-particle singlets constructed from triplets with $q_{\mathbf{l}}=q_{\mathbf{m}}=1$ and $\mathbf{l} \neq \mathbf{m}$. In turn, the perturbing terms in (1) $\propto j_{1,2}$, can be understood as a sum of operators $T_{1n,2n}$ which *nonlocally* create(destroy) $n \geq 0$ ($n < 0$) quanta within the ladder spectrum of H_0 .

It has been shown^{5,9,27,28,29} that problems of type (2) allow for perturbative analysis using a continuous unitary transformation generated by the flow equation method of Wegner³⁰. The unitarily rotated effective Hamiltonian H_{eff} reads^{27,29}

$$H_{\text{eff}} = H_0 + \sum_{n=1}^{\infty} \sum_{\substack{|\mathbf{m}|=n \\ M(\mathbf{m})=0}} C(\mathbf{m}) W_{m_1} W_{m_2} \dots W_{m_n} \quad (3)$$

where $\mathbf{m} = (m_1 \dots m_n)$ with $|\mathbf{m}| = n$ is an n -tuple of integers, each in a range of $m_i \in \{0, \pm 1, \dots, \pm N\}$ and $W_n = j_1 T_{1n} + j_2 T_{2n}$. In contrast to H of (1), H_{eff} *conserves* the total number of quanta Q . This is evident from the constraint $M(\mathbf{m}) = \sum_{i=1}^n m_i = 0$. The amplitudes $C(\mathbf{m})$ are rational numbers computed from the flow equation method^{27,29}. Explicit tabulation³¹ of the T_{in} shows that for the Hamiltonian in (1) $N=4$. In the context of spin systems the flow equation approach has been applied successfully to 1D and 2D dimer-models^{29,32}, as well as to 2D and 3D quadrumer-models^{5,9}

Q -conservation of H_{eff} leads to a ground state energy of $E_g = \langle 0 | H_{\text{eff}} | 0 \rangle$. Q -conservation also guarantees the $Q=1$ -triplets to remain genuine one-particle states, i.e., their dispersion can be calculated via $E_{\mu}(\mathbf{k}) = \sum_{lm} t_{\mu,lm} e^{i(k_x l + k_y m)}$ where $t_{\mu,lm} = \langle \mu, lm | H_{\text{eff}} | \mu, 00 \rangle - \delta_{lm,00} E_g^{obc}$ are hopping matrix elements from site $(0,0)$ to site (l,m) for a quadrumer excitation μ inserted into the unperturbed ground state. $t_{\mu,lm}$ has to be evaluated on clusters with open boundary conditions large enough to embed all linked paths of length n connecting sites $(0,0)$ to (l,m) at $O(n)$ of the perturbation. $E_g^{obc} = \langle 0 | H_{\text{eff}} | 0 \rangle$ on the $t_{\mu,00}$ -cluster. States from sectors with $Q > 1$ will not only disperse via H_{eff} but require the solution of an interacting problem.

III. ELEMENTARY TRIPLET EXCITATIONS

We have evaluated the one particle hopping matrix elements up to fifth order. They are listed explicitly in the appendix. Several of the resulting dispersions $E_T(\mathbf{k}, j_1, j_2)$ are shown in fig. 2 both, as a function of the wave vector along the irreducible wedge of the Brillouin zone of the 2D square lattice and for various values of the coupling constants j_1 and j_2 .

Two effects can be extracted from fig. 2. First, it demonstrates that the CCM 'localizes' triplet excitations on the line of largest inter-quadrumer frustration, i.e. for $j_1 = j_2$. This can be observed both, from the three panels a), b), and c) where the dispersions seem completely

flat for $j_1=j_2$, but also from the explicit expressions for t_{lm} in appendix B. I.e., up to $O(4)$ and for $l \neq m$ all hopping matrix elements are proportional to powers of $(j_1 - j_2)$. For $l \neq m$ and $lm \neq 10$ this remains true even up to $O(5)$, where however $t_{10} \neq 0$. Therefore the triplet-localization at maximum frustration is *not* complete and a weak hopping remains beyond $O(4)$. Inserting $j_1=j_2$ into (B1-B13) we find that $E_T(\mathbf{k}, j_1 = j_2)$ is exactly identical up to $O(5)$ with an $O(7)$ SE which is available for this case⁹.

The second fact to note from fig. 2 is that the VBC ground-state is unstable with respect to triplet-softening, i.e. magnetic ordering at suitably chosen values of the coupling constants. Depending on the ratio of $j_2/j_1 > 1$ or < 1 this instability will occur either at a critical wave vector of $\mathbf{k}_c = (\pi, \pi)$ or $(0, 0)$. Consistently with this the structure of exchange for the CCM, although topologically distinct, is bipartite both, for $j_1 \neq 0, j_2 \rightarrow 0$ and for $j_1 \rightarrow 0$ and $j_2 \neq 0$. The instabilities are studied in more detail in the next section.

Finally, panel a) and b) of fig. 2 contain $O(4)$ SEs for a comparison with the $O(5)$ results. The difference is small only. For j_1 and j_2 along path c) the difference is hardly visible and the $O(4)$ SE has not been displayed in the corresponding panel. The case of $j_1 = 0.5$ and $j_2 = 0$ in panel c) is identical to a particular realization of the plaquette square-lattice Heisenberg magnet. The triplet dispersion of this system has been investigated with a rather different type of fifth-order plaquette SE by Koga and Kawakami³⁴. Their result for the triplet dispersion, is included by the dots in panel c) and is in excellent agreement with our findings.

IV. QUANTUM PHASE TRANSITIONS

In the following we consider the lines of quantum phase transitions resulting from the closing of the elementary triplet-gap. This provides for an upper bound on the extent of the region of stability of the VBC in a tentative quantum phase diagram of the CCM. In principle additional first order transitions could occur or excited states other than the elementary triplets could collapse onto the ground state as well, leading to additional phase boundaries. Here we focus on the triplet instability. Moreover, we limit our discussion to AFM couplings $j_{1(2)} > 0$ and consider ferromagnetic cases elsewhere³³.

Before proceeding we stress that the CCM is *symmetric* under the interchange $j_1 \leftrightarrow j_0$ and a diagonal shift by one unit cell. This implies that the *complete* quantum phase diagram can be obtained from a mirror reflection of the region $0 < j_1 < 1$ and $0 < j_2$ at the line $(j_1 = 1, j_2)$ and a subsequent relabeling of the axis by $j_1 \rightarrow j_0/j_1 \equiv 1/j_1$ and $j_2 \rightarrow j_2/j_1$.

The results are summarized in figs. 3 and 4 which display information from the plain series as well as from a Dlog-Padé analysis. In fig. 3a) we show the evolution with increasing order of the lines of vanishing triplet gap

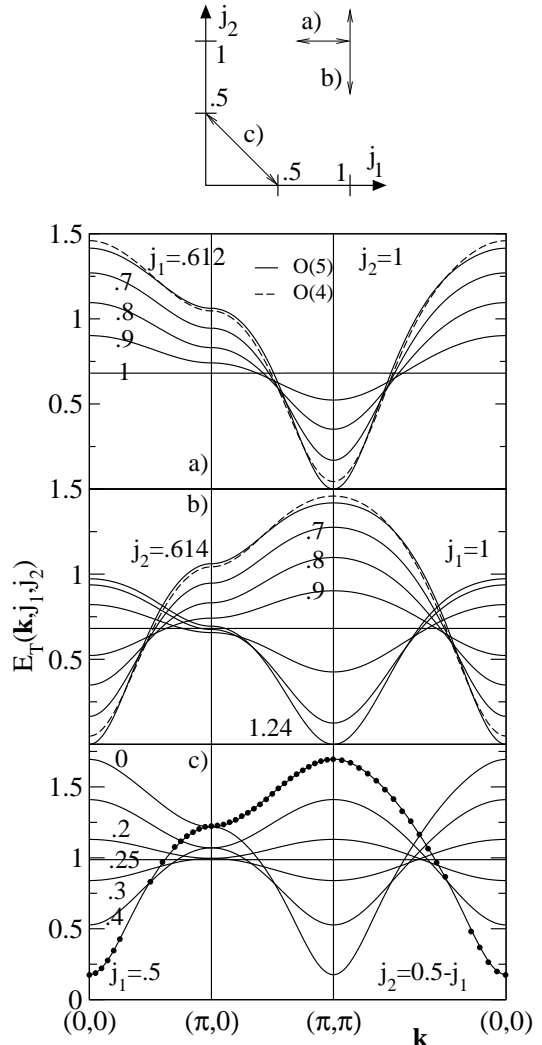


FIG. 2: Evolution of the triplet dispersion $E_T(\mathbf{k}, j_1, j_2)$ for various j_1, j_2 chosen along the directions a), b), and c) sketched in the top panel and for a path of $\mathbf{k} = (0, 0) - (\pi, 0) - (\pi, \pi) - (0, 0)$ in the 2D Brillouin zone. Solid[dashed] curves in panels a)-c)[a),b)]: $O(5)$ [$O(4)$] SEs. Dots in panel c): different $O(5)$ SE for the plaquette square-lattice from ref.³⁴.

of the *bare* series. First, this figure further clarifies the location of the critical wave-vector \mathbf{k}_c as anticipated already in fig. 2. Second the panel is intended to prove a monotonous and smooth behavior of the bare series within the range of interest. Based on the $O(5)$ SE, fig. 3b) shows the transition lines resulting from single-variable Dlog-Padés which have been obtained by parameterizing $j_{2(1)}$ of the bare SE by $j_{2(1)} = aj_{1(2)}$ for $j_{2(1)} < j_{1(2)}$. The figure displays a [2,2] and a [1,3] Dlog-Padé. They are indistinguishable on the scale of the plot. The lower(upper) critical value of j_2 which they yield for the closing of the triplet gap on the line $(j_1=1, j_2)$ are $j_2^{c_1} = 0.81$ and $j_2^{c_2} = 1.06$. As discussed in the next paragraph, along the diagonal, i.e. for $j_1=j_2$, Dlog-Padés can be obtained also from an $O(7)$ SE⁹. They result in some-

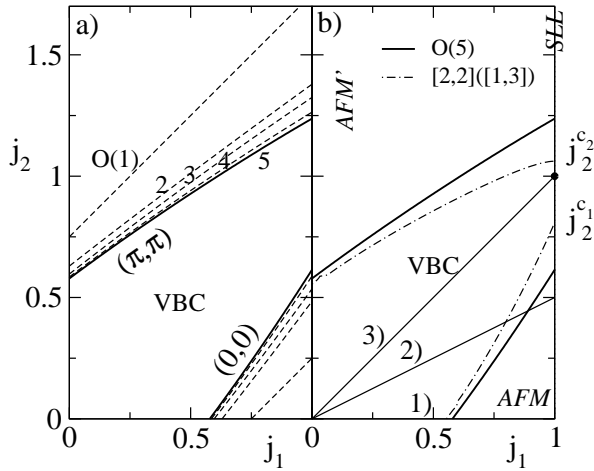


FIG. 3: Triplet instabilities of the generalized CCM: a) Lines of vanishing triplet-gap for increasing orders of the *bare* SE from $O(1)$ to $O(5)$. Triplet softening occurs at the wave vector (π, π) and $(0, 0)$ for the upper and lower set of lines. VBC labels the region of a finite triplet gap. b) Comparison of the lines of vanishing triplet-gap at $O(5)$ of the bare SE (solid) with the corresponding $[2,2]$ and $[1,3]$ Dlog-Padé approximants (dashed-dotted). The latter two are indistinguishable on the scale of the plot. Along the selected directions 1), 2) and 3) cuts from the Dlog-Padé analysis are exemplified in fig. 4. The solid dot at $j_1=j_2=1$ refers the checkerboard point. The regions labeled by italic style AFM' are likely to exhibit antiferromagnetic ordering^{11,22,35,36,37}. On the line $(j_1 = 1, j_2)$ and for $j_2 > j_2^{c2}$ the ground state is a 'sliding Luttinger liquid'^{16,17,18} (SLL). The remainder of this diagram for all coupling constants is obtained by reflection along $(j_1 = 1, j_2)$ and a rescaling of $j_1 \rightarrow 1/j_1$ and $j_2 \rightarrow j_2/j_1$ (see text).

what larger values of the critical couplings than the $O(5)$ SE. Roughly interpolating the difference in j_2^c between the $O(5)$ and $O(7)$ Dlog-Padés along this direction down to the line $(j_1=1, j_2)$ we approximate an error for the critical couplings of $j_2^{c1} = 0.79 \dots 0.81$ and $j_2^{c2} = 1.06 \dots 1.13$. These values should be contrasted against LSW theory²², which predicts stability of an AFM phase for $j_2/j_1 \leq 0.76$ at $j_1 = 1$. Moreover, ED at $j_1 = 1$ for up to 36 spins¹¹ suggests a closing of the spin-gap below $j_2/j_1 \approx 0.65$ and a crossover to 1D SLL-behavior at $j_2/j_1 \sim 1.5$.

The role of the Padé analysis in fixing the location of the quantum critical points as compared to the bare SE is clarified in more detail in fig. 4 where several reintegrated Dlog-Padés are displayed along with the plain series for three selected directions shown in fig. 3b). For $j_1 = j_2$, where the Padé analysis is expected to be most relevant, an $O(7)$ SE from ref.⁹ has been included in fig. 4.3). Because of the symmetries of the quantum phase diagram the curves beyond the vertical dashed line in fig. 4.3) do not refer to actual values of the spin gap for $j > 1$. This range is shown for completeness sake only. Most important, from fig. 4.3) one realizes that both, the plain SE as well as all of the Padé approximants yield *no* critical

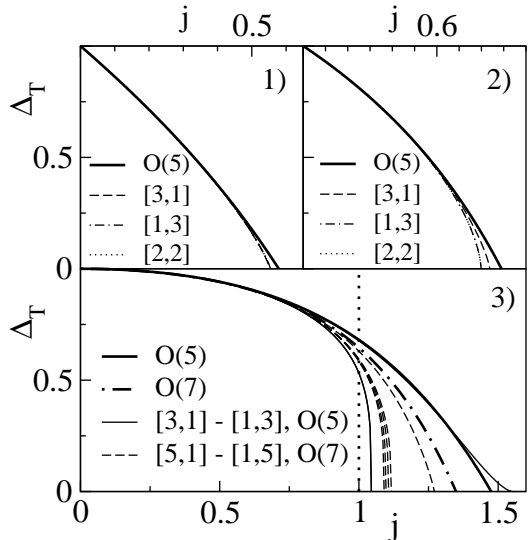


FIG. 4: Spin gap Δ_T of the bare series (thick solid and thick dashed-dotted) vs. reintegrated Dlog-Padé approximants along three selected directions 1), 2), and 3) shown in fig. 3b), i.e. $j_1 = j$ and $j_2 = aj$ with $a = 0, 0.5$ and 1 . The $O(7)$ SE in panel 3) is from ref.⁹. At $O(5)$ all (the $[2,2]$ and $[1,3]$) approximants are indistinguishable on the scale of panel 1) (2) and 3)). At $O(5)$, in panel 2) and 3) ($O(7)$, in panel 3)) the $[3,1]$ ($[5,1]$) approximant is split off from the remaining ones and is closer to the bare SE.

points for $j \leq 1$. While this agrees with earlier findings of a finite spin gap at $j = 1$ in refs.^{8,9,11} it seems that the checkerboard point is almost critical. Panel 3) shows that the $[4,2]-[1,5]$ and the $[2,2]-[1,3]$ approximants at $O(7)$ and $O(5)$, respectively, are well clustered with critical points clearly separated from those of the corresponding plain SE and the $[5,1]$ and $[3,1]$ approximants. Therefore, the Dlog-Padé analysis at $O(5)$ and arbitrary j_1, j_2 in fig. 3b) has been based on the $[2,2]$ and $[1,3]$ approximants. The effects of the Dlog-Padés in figs. 4.1) and 2) is rather minute, with the $[2,2]$ and $[1,3]$ approximants leading to essentially identical spin gaps.

As noted already, direction 1) in fig. 3b) refers to the plaquette square-lattice Heisenberg model. Its transition to the AFM state for $j \rightarrow 1$ has been studied by several groups. We may therefore compare the critical coupling $j_c = 0.555$ which we find with that obtained by other SE investigations, i.e. $j_c = 0.555$ in ref.³⁵ and $j_c = 0.54$ in ref.³⁶, as well as by ED, i.e. $j_c = 0.6$ in ref.³⁷. The agreement is satisfying.

Regarding the symmetry of the ground state in region AFM' in fig. 3b), no conclusions can be drawn from the quadrumer SE. Yet, subsuming the present work with refs.^{11,22,35,36,37} it is very likely that region AFM exhibits simple Neél-type AFM-LRO. Within AFM the CCM acquires a bipartite lattice-structure as $j_1 \rightarrow 0$ which could trigger a '4-up-4-down'-type AFM-LRO of the crossed chains for $j_2 \gtrsim 1$. The crossover between this and the SLL phase as $j_1 \rightarrow 1$ is an open issue.

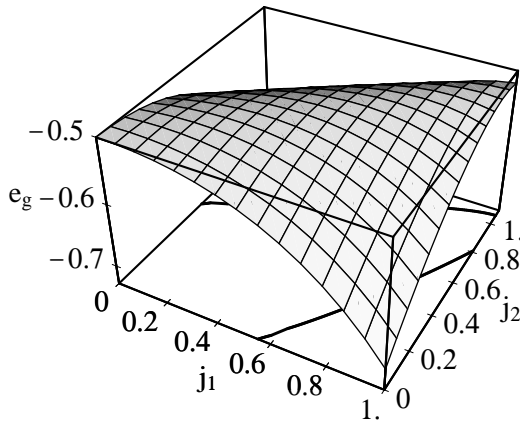


FIG. 5: $O(6)$ ground-state energy e_g per spin from eqn. (4). e_g resembles the ground-state energy of the CCM only within the range of stability of the VBC bounded by thick solid lines in the (j_1, j_2) -plane, i.e. the dashed-dotted lines from fig. 3b).

V. GROUND STATE ENERGY

To obtain SEs for the ground state energy valid to $O(n)$ in the thermodynamic limit, i.e. for systems of infinite size one may evaluate the matrix element $\langle 0 | H_{\text{eff}} | 0 \rangle$ on single 'maximal' clusters, i.e. with periodic boundary conditions and sufficiently large not to allow for wrap around at graph-length $n^9,29$. Here, Q -conservation of H_{eff} is the main ingredient which reduces the size of the intermediate Hilbert spaces. However, for the CCM we find the maximal-cluster approach to be severely limited by memory-constraints and we have combined the flow-equation approach with a linked cluster expansion. Some details of the latter are commented on in appendix A. Up to $O(6)$ the ground state energy e_g per spin is

$$\begin{aligned}
 e_g = & -\frac{1}{2} - \frac{67j_1^2}{576} - \frac{481j_1^3}{13824} - \frac{17951j_1^4}{663552} - \frac{5705977j_1^5}{522547200} \\
 & - \frac{13033565594599j_1^6}{2123765592883200} + \frac{2j_1j_2}{9} + \frac{59j_1^2j_2}{1728} + \frac{224267j_1^3j_2}{4354560} \\
 & + \frac{388714973j_1^4j_2}{35115171840} + \frac{655905584767j_1^5j_2}{130026464870400} - \frac{67j_2^2}{576} \\
 & + \frac{59j_1j_2^2}{1728} - \frac{4837781j_1^2j_2^2}{104509440} + \frac{75848383j_1^3j_2^2}{175575859200} \\
 & - \frac{169095132323j_1^4j_2^2}{168552824832000} - \frac{481j_2^3}{13824} + \frac{574241j_1j_2^3}{13063680} \\
 & + \frac{38923349j_1^2j_2^3}{58525286400} + \frac{113410023666229j_1^3j_2^3}{15928241946624000} - \frac{139031j_2^4}{5971968} \\
 & + \frac{1184653457j_1j_2^4}{175575859200} - \frac{65325840449533j_1^2j_2^4}{10618827964416000} - \frac{2624063j_2^5}{313528320} \\
 & + \frac{181444615182347j_1j_2^5}{31856483893248000} - \frac{51497150603363j_2^6}{10618827964416000} \quad (4)
 \end{aligned}$$

First we note, that at the checkerboard point, i.e. for $j_1 = j_2$ eqn. (4) is identical to the corresponding SE for e_g in eqn. (6) of ref.⁹. Figure 5 visualizes e_g , resem-

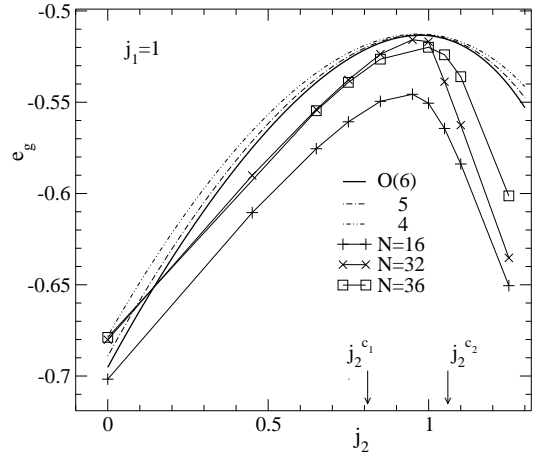


FIG. 6: Ground state energy of the CCM on the line ($j_1 = 1, j_2$). Thick solid, dashed-dotted, and dashed-double-dotted lines: SE. Solid curves with symbols: ED from fig. 2 of ref.¹¹. $j_2^{c1(2)}$ critical couplings from Dlog-Padé at $O(5)$, see fig. 3b).

bling a convex function with the weakest energy gain in the vicinity of the line of strongest frustration, i.e. for $j_1 = j_2$. Note, that fig. 5 is the ground state energy of the CCM only within the region of stability of the VBC. Obviously e_g is below the ground state energy of the bare quadrumer limit for all j_1, j_2 . This is consistent with refs.^{8,9,11} and is at variance with a 'tetrahedral' SE to $O(3)$ at $j_1=j_2$ in ref.²⁶, where $e_g > -0.5$ has been found.

In ref.⁹ it has been shown, that e_g at $j_1=j_2$ agrees to within 1% with that of ED on systems with 36 spins for $j_1 \leq 1$. In fig. 6 we compare e_g with ED-results along the line ($j_1 = 1, j_2$) obtained by Sindzingre, Fouet, and Lhuillier¹¹ for systems with 16, 32, and 36 spins. The SE is displayed along with its variation in going from $O(4)$ to $O(6)$ in order to provide a rough estimate of convergence. As with fig. 5 the SE resembles the actual ground state energy only within the range of critical couplings $j_2^{c1(2)}$ marked on the j_2 -axis. While the line ($j_1=1, j_2$) is rather remote from the limit of decoupled quadrumer, the agreement between SE and ED on the largest system depicted in fig. 6 is still satisfying - even below j_2^{c1} .

Finally, one may define a 'point of maximum frustration', i.e. j_2^{mf} at maximum e_g for $j_1=1$. Interestingly $j_2^{mf} \neq 1$, i.e. it is off from the checkerboard point. We find that $j_2^{mf} \approx 0.973 \pm 0.004$. The error has been approximated from twice the difference between j_2^{mf} at $O(5)$ and $O(6)$. As similar observation has been reported in ref.¹¹.

VI. CONCLUSION

To summarize, we have investigated the ground state properties and the elementary triplet excitations of the generalized crossed-chain quantum-spin model by quadrumer series expansion. Over a large region of exchange parameters the model exhibits a finite spin

gap which is smoothly connected to the limit of the bare quadrumer. This region is bounded by lines of triplet softening which results from a delocalization of the triplets away from the case of complete frustration of the inter-quadrumer exchange. This remains true in particular not only at – but also in the vicinity of the checkerboard point for $j_1=1$ where we have established a finite range of on-chain exchange, i.e. $0.79...0.81 \lesssim j_2 \lesssim 1.06...1.13$ with a non-zero spin gap. While the fate of more complex multiparticle excitations as a function of $j_{1(2)}$ remains to be investigated in the future, our findings are consistent with a ground-state symmetry in the region of non-zero spin gap identical to that at $j_{1(2)}=0$, i.e. a valence-bond-solid.

Acknowledgments - It is a pleasure to thank A. Honecker for fruitful discussions and D. C. Cabra for helpful comments on SLLs. This research was supported in part by the Deutsche Forschungsgemeinschaft, Schwerpunktprogramm 1073, under Grant No. BR 1084/2-3.

APPENDIX A: LINKED CLUSTER EXPANSION

Here we comment on a peculiarity of graph counting for the quadrumer expansion for the CCM as compared to that for standard expansions for spin lattice-models with no internal structure of the vertices and edges. For the latter, both pairs of graphs in fig. 7a) and b) are isomorphic and yield identical results. In general this is *not* the case for the quadrumer expansion. This is due to the vertices(edges) to consist of 4-spin quadrumer(tetrahedral links) which prohibit ‘free rotation’ of a graph at its vertices. Similarly, ‘twisting’ of an edge - as for edge ‘e’ in fig. 7b) - is *no* symmetry operation in general. In fact, this depends on the choice of parameters, i.e. exactly at the checkerboard point, for $j_1=j_2$, the tetrahedral link is symmetric under the twist. This is reflected in, the corresponding cluster weights for the ground state energies, which (discarding lattice constants) read

$$\begin{aligned} \text{Graph 1b)} = & -\frac{8597351609683j_1^6}{6371296778649600} + \\ & \frac{9198603350203j_1^5j_2}{1327353495552000} - \frac{473964630567761j_1^4j_2^2}{31856483893248000} + \\ & \frac{1700981391083j_1^3j_2^3}{94810963968000} - \frac{143988201852347j_1^2j_2^4}{10618827964416000} + \\ & \frac{23692204192849j_1j_2^5}{3982060486656000} - \frac{7166568732467j_2^6}{6371296778649600} \quad (\text{A1}) \end{aligned}$$

$$\begin{aligned} \text{Graph 2b)} = & -\frac{7166568732467j_1^6}{6371296778649600} + \\ & \frac{23692204192849j_1^5j_2}{3982060486656000} - \frac{143988201852347j_1^4j_2^2}{10618827964416000} \\ & + \frac{1700981391083j_1^3j_2^3}{94810963968000} - \frac{473964630567761j_1^2j_2^4}{31856483893248000} + \\ & \frac{9198603350203j_1j_2^5}{1327353495552000} - \frac{8597351609683j_2^6}{6371296778649600} \quad (\text{A2}) \end{aligned}$$

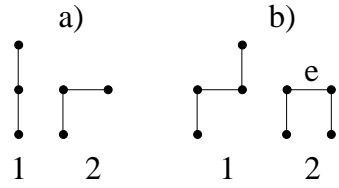


FIG. 7: Non-isomorphic (isomorphic) graphs of the quadrumer (standard) expansion on the crossed-chain (simple square) lattice. Graph 2 is meant to result from 1 by: a) an *in-plane* 90° rotation of the upper edge, b) a 180° -*out-of-plane* rotation of the upper edge around edge ‘e’.

Only if $j_1=j_2$ eqns. A1 and A2 are identical. In conclusion, the number of non-isomorphic graphs in the quadrumer expansion for the CCM is significantly larger than that in standard expansions for 2D square-lattice models.

APPENDIX B: TRIPLET HOPPING AMPLITUDES

In this appendix, and for completeness sake, we list the triplet dispersion $E_T(\mathbf{k})$ in the thermodynamic limit up to $O(j_1^m, j_2^n)$ with $m + n \leq 5$ which can be written as

$$\begin{aligned} E_T(\mathbf{k}, j_1, j_2) = & t_{00} + \\ & t_{10}(\cos(k_x) + \cos(k_y)) + \\ & t_{11} \cos(k_x) \cos(k_y) + \\ & t_{20}(\cos(2k_x) + \cos(2k_y)) + \\ & t_{21}(\cos(2k_x) \cos(k_y) + \cos(k_x) \cos(2k_y)) + \\ & t_{22} \cos(2k_x) \cos(2k_y) + \\ & t_{30}(\cos(3k_x) + \cos(3k_y)) + \\ & t_{31} \cos(k_x) \cos(k_y)(\cos(2k_x) + \cos(2k_y) - 1) + \\ & t_{32}(\cos(3k_x) \cos(2k_y) + \cos(2k_x) \cos(3k_y)) + \\ & t_{40}(\cos(4k_x) + \cos(4k_y)) + \\ & t_{41}(\cos(4k_x) \cos(k_y) + \cos(k_x) \cos(4k_y)) + \\ & t_{50}(\cos(5k_x) + \cos(5k_y)) \quad (\text{B1}) \end{aligned}$$

where the hopping amplitudes t_{00}, \dots, t_{50} are given by

$$\begin{aligned} t_{00} = & 1 + \frac{145j_1^2}{432} + \frac{2771j_1^3}{13824} + \frac{9633109j_1^4}{34836480} + \\ & \frac{440341849993j_1^5}{2106910310400} - \frac{187j_1j_2}{216} - \frac{1033j_1^2j_2}{4608} - \\ & \frac{281352751j_1^3j_2}{313528320} - \frac{173134656371j_1^4j_2}{300987187200} + \frac{145j_2^2}{432} - \\ & \frac{1033j_1j_2^2}{4608} + \frac{30651767j_1^2j_2^2}{26127360} + \frac{13833647581j_1^3j_2^2}{35115171840} + \\ & \frac{2771j_2^3}{13824} - \frac{90015077j_1j_2^3}{104509440} + \frac{5030806153j_1^2j_2^3}{19508428800} + \\ & \frac{81044221j_2^4}{313528320} - \frac{50889983953j_1j_2^4}{100329062400} + \frac{411234777481j_2^5}{2106910310400} \quad (\text{B2}) \end{aligned}$$

$$\begin{aligned}
t_{10} = & (j_1 - j_2) \left(-\frac{1}{3} - \frac{j_1}{18} + \frac{29827j_1^2}{497664} + \frac{1511209j_1^3}{39813120} - \right. \\
& \frac{j_2}{18} - \frac{37667j_1j_2}{248832} - \frac{5805011j_1^2j_2}{119439360} + \frac{12673j_2^2}{165888} - \\
& \left. \frac{1265911j_1j_2^2}{23887872} + \frac{4947067j_2^3}{119439360} \right) + \\
& \frac{562865130343j_1^5}{6320730931200} - \frac{4144974245353j_1^4j_2}{12641461862400} + \\
& \frac{2307417015943j_1^3j_2^2}{4213820620800} - \frac{485959984667j_1^2j_2^3}{842764124160} + \\
& \frac{1577116657219j_1j_2^4}{4213820620800} - \frac{672640186583j_2^5}{6320730931200} \quad (B3)
\end{aligned}$$

$$\begin{aligned}
t_{11} = & 4(j_1 - j_2) \left(-\frac{j_1}{9} - \frac{7j_1^2}{162} + \frac{1221199j_1^3}{89579520} + \right. \\
& \frac{705849089j_1^4}{25082265600} + \frac{j_2}{9} - \frac{3836587j_1^2j_2}{29859840} - \frac{23977237j_1^3j_2}{214990848} + \\
& \frac{7j_2^2}{162} + \frac{1199609j_1j_2^2}{9953280} + \frac{20880367j_1^2j_2^2}{3135283200} - \frac{507919j_2^3}{89579520} + \\
& \left. \frac{39361331j_1j_2^3}{358318080} - \frac{2514549451j_2^4}{75246796800} \right) \quad (B4)
\end{aligned}$$

$$\begin{aligned}
t_{20} = & 2(j_1 - j_2)^2 \left(-\frac{1}{54} - \frac{125j_1}{5184} - \frac{5789171j_1^2}{179159040} - \right. \\
& \frac{2583021851j_1^3}{120394874880} - \frac{125j_2}{5184} + \frac{57485j_1j_2}{17915904} - \\
& \frac{176614487j_1^2j_2}{85996339200} - \frac{5789171j_2^2}{179159040} - \frac{62829919j_1j_2^2}{9555148800} - \\
& \left. \frac{11680356743j_2^3}{601974374400} \right) \quad (B5)
\end{aligned}$$

$$\begin{aligned}
t_{21} = & 4(j_1 - j_2)^2 \left(-\frac{23j_1}{486} - \frac{875j_1^2}{31104} - \right. \\
& \frac{528075769j_1^3}{56435097600} + \frac{j_2}{18} - \frac{49j_1j_2}{116640} - \frac{13388351j_1^2j_2}{391910400} + \\
& \left. \frac{11j_2^2}{384} + \frac{3859528429j_1j_2^2}{112870195200} + \frac{320776609j_2^3}{37623398400} \right) \quad (B6)
\end{aligned}$$

$$\begin{aligned}
t_{22} = & 4(j_1 - j_2)^2 \left(-\frac{103j_1^2}{2916} - \frac{258601j_1^3}{8398080} + \right. \\
& \frac{317j_1j_2}{4374} + \frac{1457333j_1^2j_2}{41990400} - \frac{293j_2^2}{8748} + \\
& \left. \frac{1207837j_1j_2^2}{41990400} - \frac{266113j_2^3}{8398080} \right) \quad (B7)
\end{aligned}$$

$$\begin{aligned}
t_{30} = & 2(j_1 - j_2)^2 \left(-\frac{j_1}{54} - \frac{1849j_1^2}{466560} - \right. \\
& \frac{1692644279j_1^3}{56435097600} + \frac{j_2}{54} + \frac{9653478197j_1^2j_2}{112870195200} + \\
& \frac{1849j_2^2}{466560} - \frac{10100761397j_1j_2^2}{112870195200} + \\
& \left. \frac{1870410679j_2^3}{56435097600} \right) \quad (B8)
\end{aligned}$$

$$\begin{aligned}
t_{31} = & 8(j_1 - j_2)^3 \left(-\frac{31j_1}{1458} - \frac{838229j_1^2}{41990400} + \frac{j_2}{54} + \right. \\
& \left. \frac{7927j_1j_2}{3499200} + \frac{871649j_2^2}{41990400} \right) \quad (B9)
\end{aligned}$$

$$\begin{aligned}
t_{32} = & 4(j_1 - j_2)^2 \left(-\frac{2131j_1^3}{78732} + \frac{247j_1^2j_2}{2916} - \right. \\
& \left. \frac{2347j_1j_2^2}{26244} + \frac{845j_2^3}{26244} \right) \quad (B10)
\end{aligned}$$

$$\begin{aligned}
t_{40} = & 2(j_1 - j_2)^4 \left(-\frac{23}{17496} - \frac{497953j_1}{83980800} - \right. \\
& \left. \frac{497953j_2}{83980800} \right) \quad (B11)
\end{aligned}$$

$$t_{41} = 4(j_1 - j_2)^4 \left(-\frac{637j_1}{52488} + \frac{773j_2}{52488} \right) \quad (B12)$$

$$t_{50} = -\frac{161(j_1 - j_2)^5}{26244} \quad (B13)$$

- ¹ C. Lhuillier and G. Misguich, "Frustrated quantum magnets", published in Springer Series: Lecture Notes in Physics, Vol. 595, pgs. 161-190 (2002), Springer Verlag, (C. Berthier, L. P. Levy and G. Martinez Eds.).
- ² M. Hase, I. Terasaki, and K. Uchinokura, Phys. Rev. Lett. **70**, 3651 (1993).
- ³ H. Kageyama, M. Nishi, N. Aso, K. Onizuka, T. Yoshihama, K. Nukui, K. Kodama, K. Kakurai, and Y. Ueda, Phys. Rev. Lett. **84**, 5876 (2000).
- ⁴ P. Lemmens, K.-Y. Choi, E.E. Kaul, Ch. Geibel, K. Becker, W. Brenig, R. Valenti, C. Gros, M. Johnsson, P. Millet, and F. Mila, Phys. Rev. Lett. **87**, 227201 (2001).
- ⁵ W. Brenig, Phys. Rev. B **67**, 064402 (2003).
- ⁶ P. Lecheminant, B. Bernu, C. Lhuillier, L. Pierre, and P.

Sindzingre, Phys. Rev. B **56**, 2521 (1997); C. Waldtmann, H.U. Everts, B. Bernu, C. Lhuillier, P. Sindzingre, P. Lecheminant, and L. Pierre, EPJ B **2** 501 (1998).

- ⁷ F. Mila, Eur. J. Phys. **21**, 499 (2000).
- ⁸ J.-B. Fouet, M. Mambrini, P. Sindzingre, and C. Lhuillier, Phys. Rev. B **67**, 054411 (2003).
- ⁹ W. Brenig und A. Honecker, Phys. Rev. B **65**, 140407 (2002).
- ¹⁰ B. Canals, Phys. Rev. B **65**, 184408 (2002).
- ¹¹ P. Sindzingre, J.-B. Fouet, and C. Lhuillier, Phys. Rev. B **66**, 174424 (2002).
- ¹² A. Koga and N. Kawakami, Phys. Rev. B **63**, 144432 (2001).
- ¹³ H. Tsunetsugu, J. Phys. Soc. Japan **70**, 640 (2001).

¹⁴ H. Tsunetsugu, Phys. Rev. B **65**, 024415 (2002).

¹⁵ E. Berg, E. Altman, and A. Auerbach, Phys. Rev. Lett. **90**, 147204 (2003).

¹⁶ V.J. Emery, E. Fradkin, S.A. Kivelson, and T.C. Lubensky, Phys. Rev. Lett. **85**, 2160 (2000).

¹⁷ A. Vishwanath and D. Carpentier, Phys. Rev. Lett. **86**, 676 (2001).

¹⁸ O.A. Starykh, R.R.P. Singh, and G.C. Levine, Phys. Rev. Lett. **88**, 167203 (2002).

¹⁹ O. P. Sushkov, J. Oitmaa, and Z. Weihong, Phys. Rev. B **63**, 104420 (2001).

²⁰ S. Sachdev and K. Park, Ann. Phys. (N.Y.) 298, 58 (2002)

²¹ S.E. Palmer and J.T. Chalker, Phys. Rev. B **64**, 94412 (2001).

²² R.R.P. Singh, O.A. Starykh, and P.J. Freitas, J. Appl. Phys. **83**, 7387 (1998).

²³ E.H. Lieb and P. Schupp, Phys. Rev. Lett. **83**, 5362 (1999).

²⁴ R. Moessner, O. Tchernyshyov, and S.L. Sondhi, preprint cond-mat/0106286.

²⁵ O. Tchernyshyov, O. A. Starykh, R. Moessner, and A. G. Abanov, preprint cond-mat/0301303.

²⁶ M. Elhajal, B. Canals and C. Lacroix, Can. J. Phys. **79**, 1353 (2001).

²⁷ J. Stein, J. Stat. Phys. **88**, 487 (1997).

²⁸ A. Mielke, Eur. Phys. J. B **5**, 605 (1998).

²⁹ C. Knetter and G.S. Uhrig, Eur. Phys. J. B **13**, 209 (2000).

³⁰ F. Wegner, Ann. Physik **3**, 77 (1994).

³¹ On appearance of this paper additional results are available on request from the authors. These results are too lengthy to be displayed in written form but will be made available electronically.

³² E. Müller-Hartmann, R.R.P. Singh, C. Knetter, and G. S. Uhrig, Phys. Rev. Lett. **84**, 1808 (2000).

³³ W. Brenig, unpublished.

³⁴ A. Koga, N. Kawakami, preprint, cond-mat/9908458

³⁵ R.R.P. Singh, Z. Weihong, C.J. Hamer, and J. Oitmaa, Phys. Rev. B **60**, 7278 (1999).

³⁶ A. Koga, S. Kumada, and N. Kawakami, J. Phys. Soc. Jpn. **68**, 642 (1999).

³⁷ A. Voigt, Comp. Phys. Commun. **146**, 125 (2002).